Angewandte Chemie
Eine Zeitschrift der Gesellschaft Deutscher Chemiker

Supporting Information

69451 Weinheim, Germany

Supporting Information

"Li-Doped 3D Covalent Organic Frameworks: High Capacity Hydrogen Storage Materials"

Dapeng Cao [1], Jianhui Lan [1], Wenchuan Wang [1*] and Berend Smit [2*]

[1] Division of Molecular and Materials Simulation, Key Lab for Nanomaterials, Ministry of Education of China, Beijing University of Chemical Technology, Beijing 100029, China

[2] Department of Chemical Engineering and Department of Chemistry, University of California, Berkeley, California 94720-1462

* Email: wangwc@mail.buct.edu.cn; Berend-Smit@Berkeley.edu

The multiscale theoretical method used in this work combines the first-principles calculation and grand canonical Monte Carlo (GCMC) simulation to predict adsorption capacity of hydrogen in covalent organic frameworks (COFs)[1] and Li-doped COFs. This supporting file presents the details of our first-principles calculations and some additional isotherms for hydrogen adsorption in COFs by using GCMC simulations.

S.1. First-principles calculations

The crystalline 3D COFs (termed COF-102, COF-103, COF-105, and COF-108) were synthesized by self-condensation and co-condensation reactions of the rigid molecular building blocks, tetrahedral tetra(4-dihydroxyborylphenyl)methane (TBPM), and its silane analog (TBPS), and triangular hexahydroxytriphenylene (HHTP).[1] Table S1 lists the structural information of COFs derived from experimental data. [1]

To obtain the interaction between Ar and H_2 with COFs, all the first-principles calculations were implemented with the Gaussian 03 program package.[2]

Table S1 Unit cell parameters, mass, density and free volumes of 3D COFs[1]

materials	a=b=c (Å)	mass (g/mol)	density (g/cm^3)	free volume[a] (%)
COF-102	27.1771	5083.69	0.41	71.12
COF-103	28.2477	5276.59	0.38	73.25
COF-105	44.8860	9600.52	0.18	88.22
COF-108	28.4010	2351.91	0.17	88.84

[a] The free volume is the accessible volume of H_2 within one unit cell. It is accessible if the potential energy of the interaction between H_2 and the solid framework is less than 10^4 K.

S.1.1 Adsorption Sites of Hydrogen on COFs

The adsorption sites of hydrogen on COFs were first investigated with the cluster model method. In this work, several cluster models were adopted to represent the COFs. The geometry optimization was performed at the theoretical level of B3LYP/6-31G*, which gives quite accurate geometric features[3, 4]. The binding energies (B.E.) between H_2 and the studied cluster models were calculated with the PW91 exchange correlation function[5] as well as the 6-311G* basis set, based on the optimized adsorption geometries obtained above. This combined method is widely used in the first-principles calculations especially for high quality calculations.

The structures of the cluster models were frozen during geometry optimizations. The binding energy is defined as

$$\text{B.E.} = E(H_2/\text{cluster}) - E(\text{cluster}) - E(H_2).$$

The optimized geometries and binding energies for H_2 adsorption on different adsorption sites of COFs are shown in Figure S1. The binding energies for H_2 adsorption on the hydrocarbon rings of COF-102 and COF-103 are -0.701 and -0.689 kcal/mol, respectively, while -0.244 kcal/mol for H_2 on B_3O_3 rings. These results show that H_2, adsorbed in

COF-102 and COF-103, prefers to stay on the hydrocarbon rings rather than the B_3O_3 rings. Figure S1 (d) and (e) show that, when H_2 is located on the HHTP building block in COF-105 or COF-108, it prefers to stay on the top of the outer three hydrocarbon rings (B.E. = -0.813 kcal/mol) rather than the center ring (B.E. = -0.455 kcal/mol). In addition, if H_2 is located on the top of the C_2O_2B ring, it will migrate to one side of the C_2O_2B ring after optimizations with the binding energy of -0.979 kcal/mol.

.

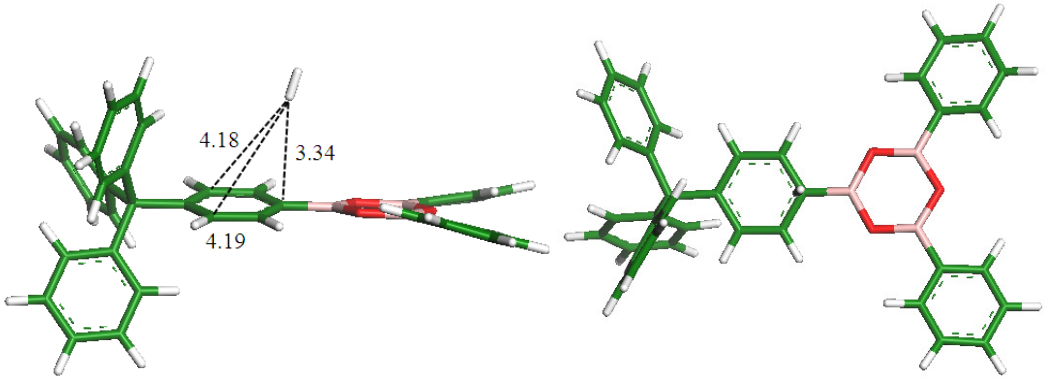

(a) B.E. = -0.701 kcal/mol

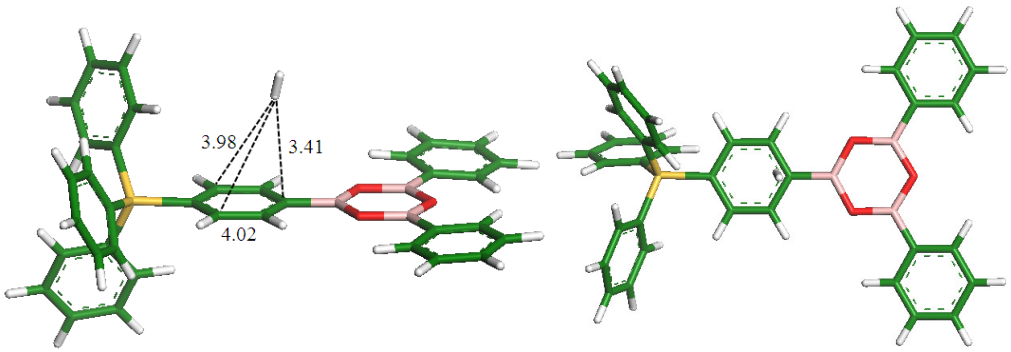

(b) B.E. = -0.689 kcal/mol

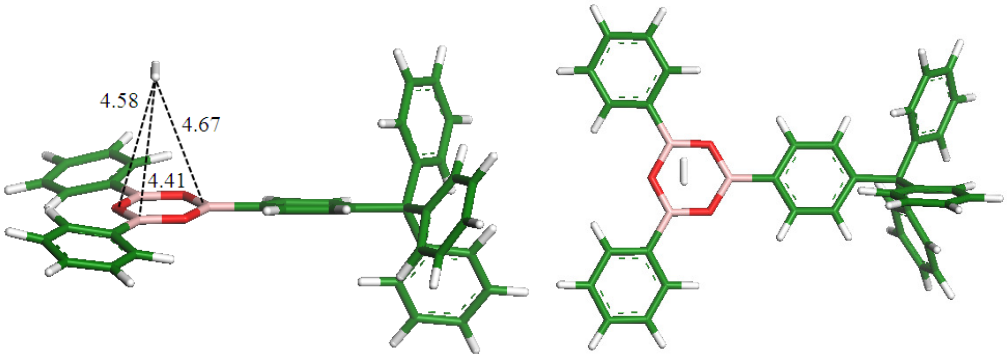

(c) B.E. = -0.244 kcal/mol

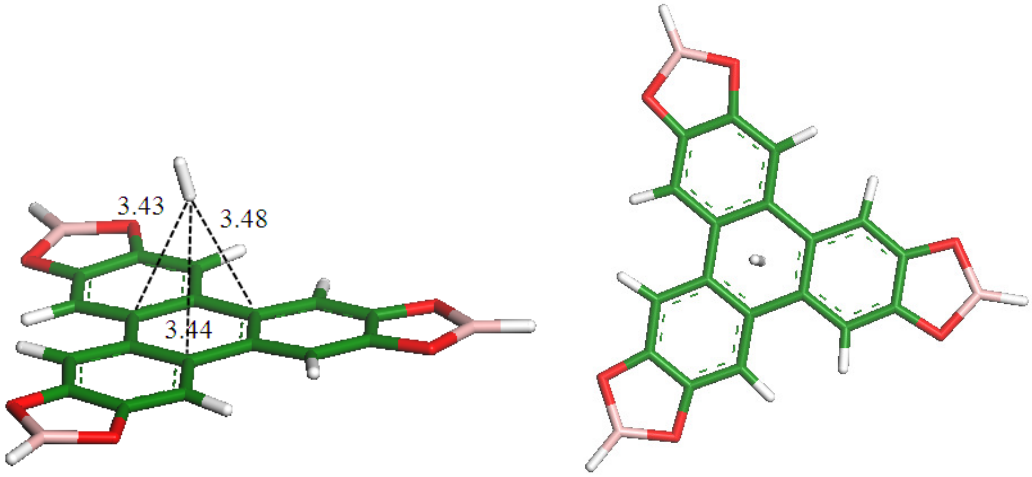

(d) B.E. = -0.455 kcal/mol

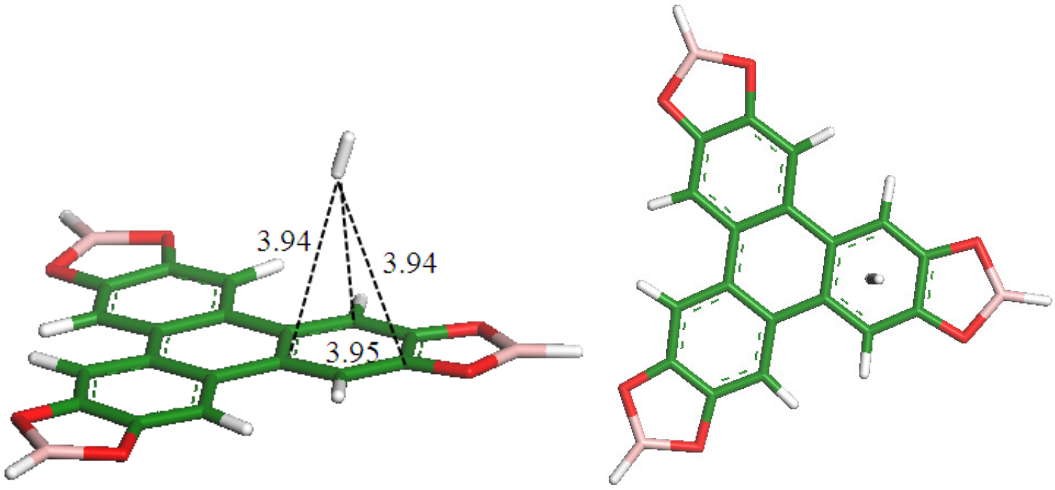

(e) B.E. = -0.813 kcal/mol

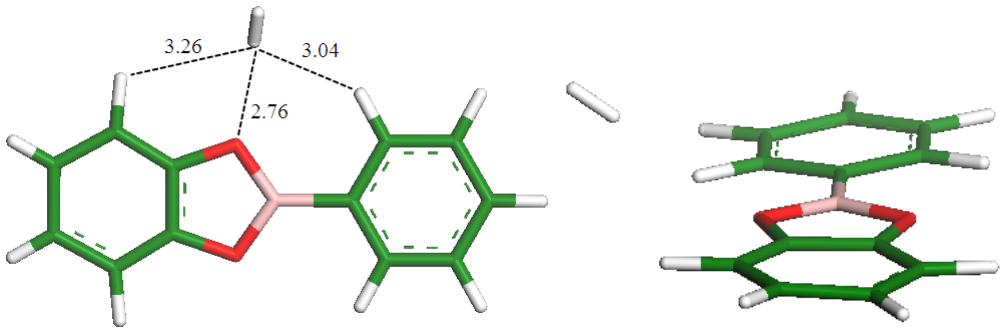

(f) B.E. = -0.979 kcal/mol

Figure S1 Optimized adsorption sites for H_2 on the fragments of COFs. White, green, pink, red and yellow denote H, C, B, O and Si, respectively.

S.1.2 Interaction of Ar and H_2 with COFs

The COF materials are mainly composed of six-membered hydrocarbon rings, six-membered B_3O_3 rings or five-membered C_2O_2B rings, and sp^3 hybridized C and Si atoms. To obtain the interaction of Ar and H_2 with COFs, four cluster models (see Figure S2) were constructed here to represent the atom types in the COFs. The interaction energies of Ar and H_2 with the four cluster models were calculated in the framework of Møller-Plesset second-order perturbation theory (MP2)[6-9] with the basis set of cc-PVTZ[10, 11]. The basis set superposition error has already been evaluated here, and our results show that this error has neglectable effect to the fitted force fields as presented in the following S.2. The above first-principles theoretical method is expected to give more reliable predictions than other levels of method. The calculated first-principles results were then used to determine the non-bond interactions, such as H-C, H-B, H-O, H-Si. Based on our previous calculations, the H_2 molecule prefers to be adsorbed on the top of C_6H_6 with its axis vertical to the plane, while on the top of $B_3O_3H_3$ with its axis parallel to the plane. Therefore, these adsorption orientations of H_2 were adopted in our potential energy

calculations as presented in Figure S6 (c) and (d), as well as for the fitting of force fields. However, for comparison we also calculated the potential energy of H_2 on C_6H_6 and $B_3O_3H_3$ with unpopular orientations as shown in Figure S6 (e) and (f). The detailed discussion was presented in S.2.

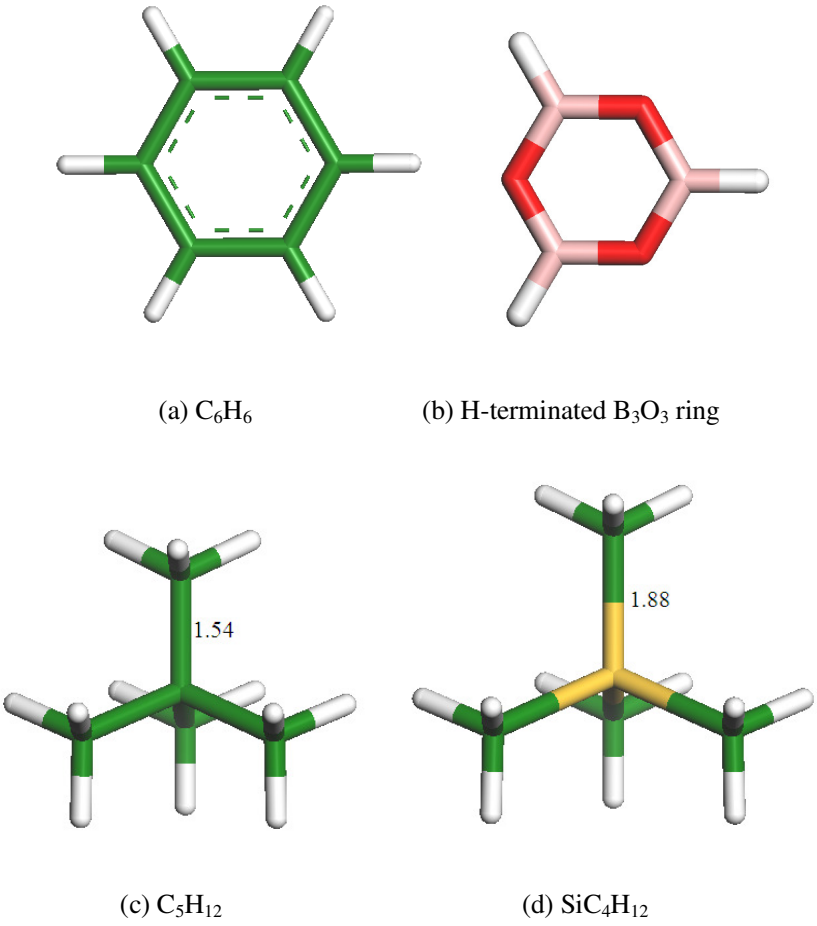

(a) C_6H_6 (b) H-terminated B_3O_3 ring

(c) C_5H_{12} (d) SiC_4H_{12}

Figure S2 Cluster models used to represent the atom types in COFs. White, green, pink, red and yellow denote H, C, B, O and Si, respectively. (a) and (b) represent the hydrocarbon rings and B_3O_3 rings in COFs. (c) and (d) are used to describe the sp^3 hydrized C and Si. Here, we assume that the H atoms in all the four cluster models belong to one atom type.

S.1.3 Interaction of Li with COFs

To improve the storage capacity of hydrogen, Goddard and co-workers[11] recommended that doping electropositive metals into MOFs might be a good strategy.[12]

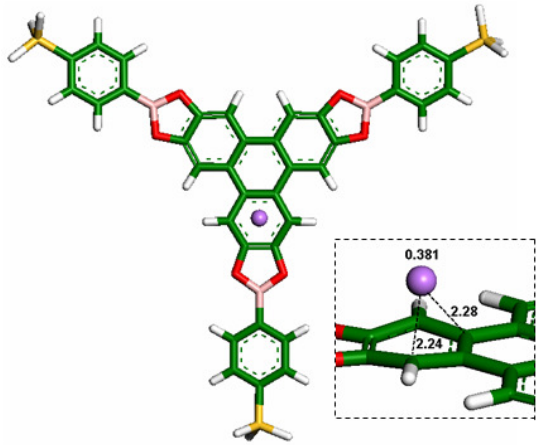

(a) Hollow site in HHTP

B.E. = -14.47 kcal/mol

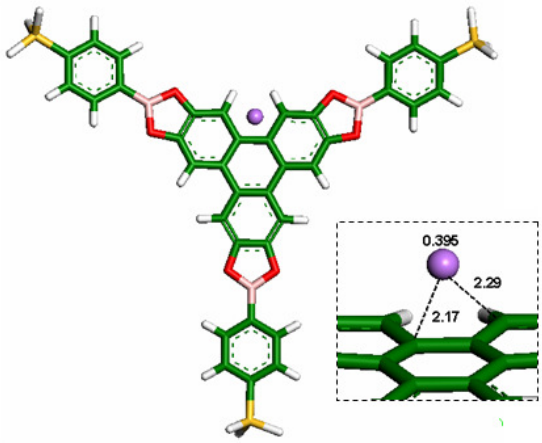

(b) Open-hollow site in HHTP

B.E. = -14.71 kcal/mol

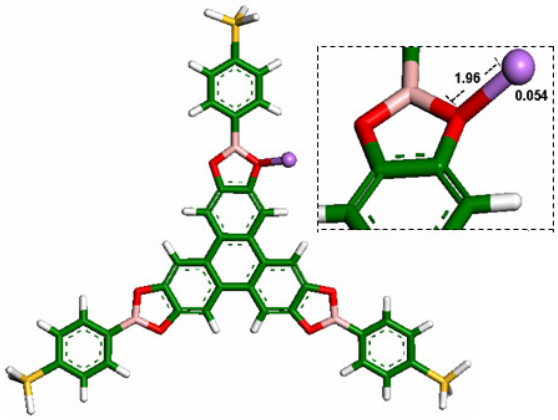

(c) Oxygen site in C_2O_2B ring

B.E. = -8.87 kcal/mol

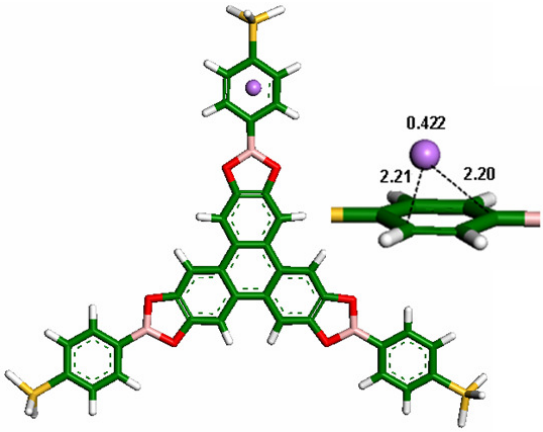

(d) Hollow site in TBPS

B.E. = -23.70 kcal/mol

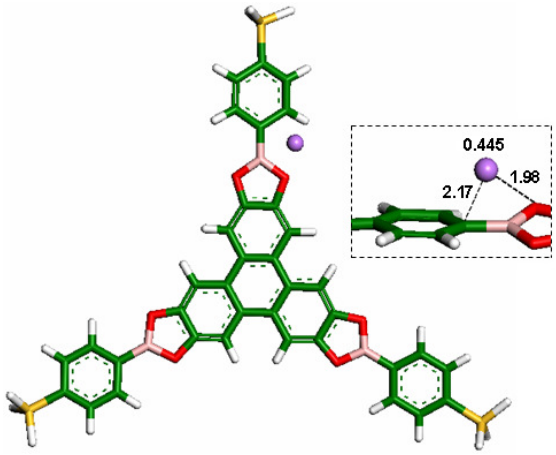

(e) Open-hollow site in TBPS
B.E. = -16.16 kcal/mol

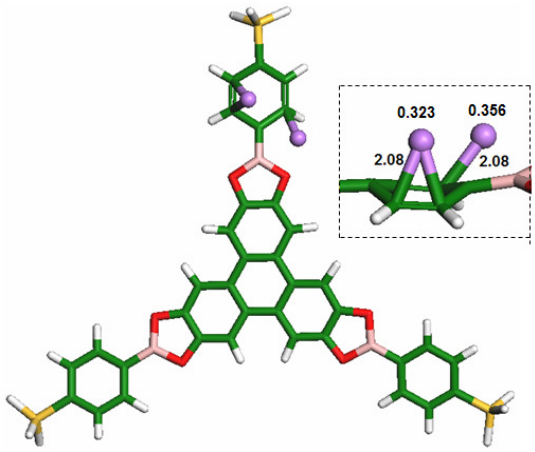

(f) Coadsorption of two Li atoms in TBPS
B.E.= -23.30 kcal/mol

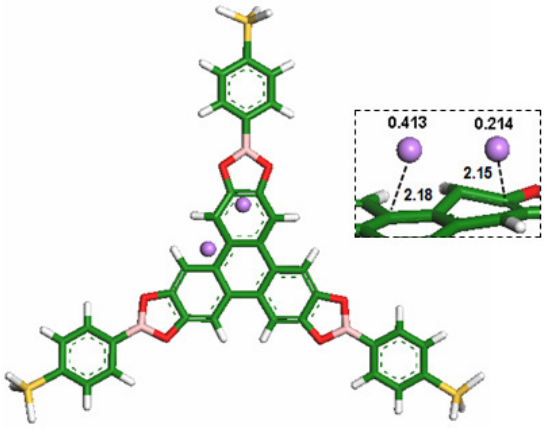

(g) Coadsorption of two Li atoms in HHTP

B.E.= -20.38 kcal/mol

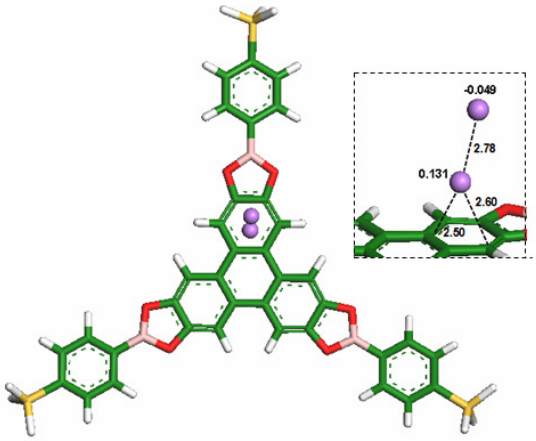

(h) Coadsorption of two Li atoms in HHTP

B.E.= -15.78 kcal/mol

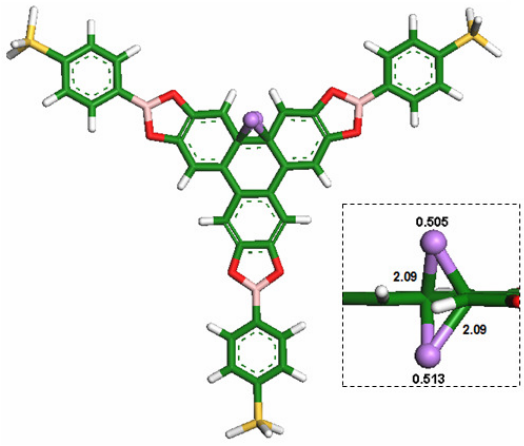

(i) Coadsorption of two Li atoms in HHTP

B.E.= -20.35 kcal/mol

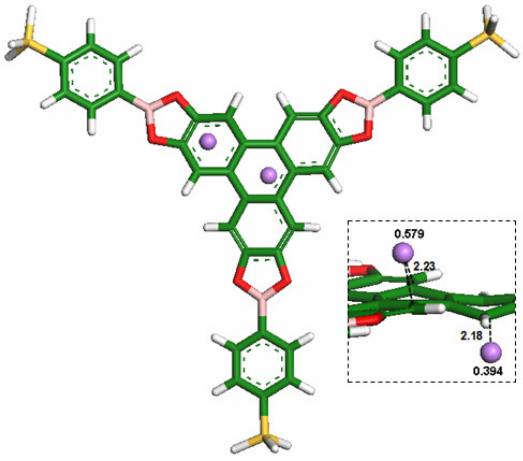

(j) Coadsorption of two Li atoms in HHTP

B.E.= -17.35 kcal/mol

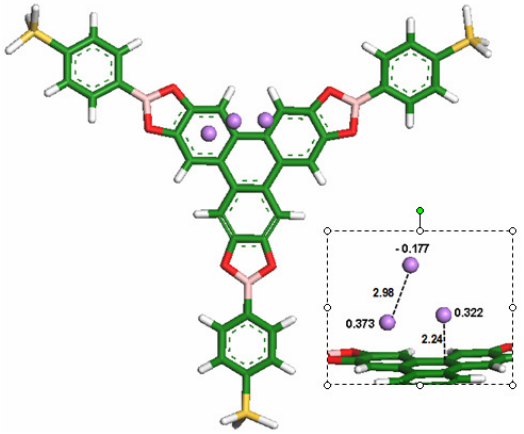

(k) Coadsorption of three Li atoms in HHTP

B.E.= -33.75 kcal/mol

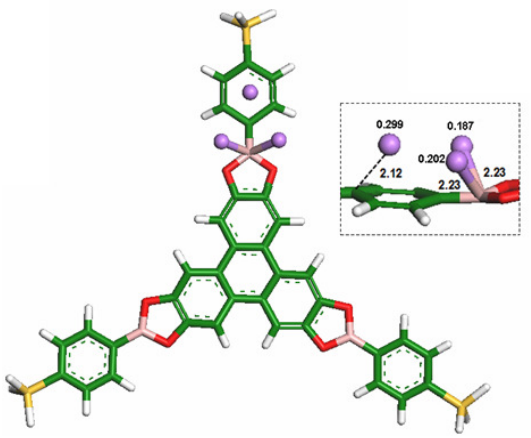

(l) Coadsorption of three Li atoms in TBPS

B.E.= -38.16 kcal/mol

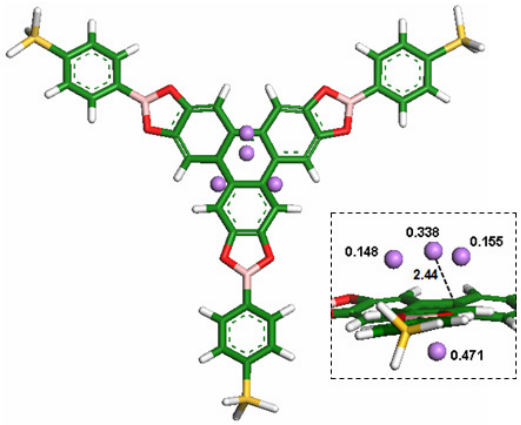

(m) Coadsorption of four Li atoms in HHTP

B.E.= -38.02 kcal/mol

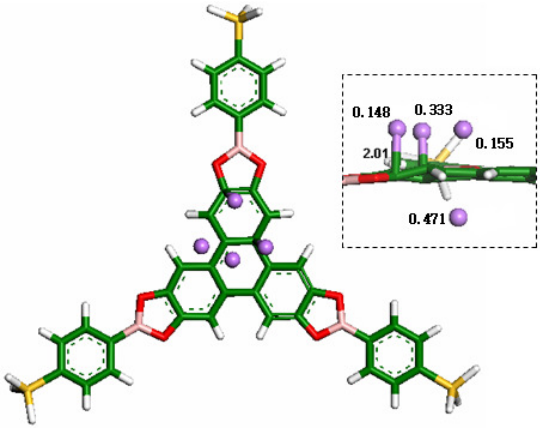

(n) Coadsorption of four Li atoms in HHTP

B.E.= - 44.99 kcal/mol

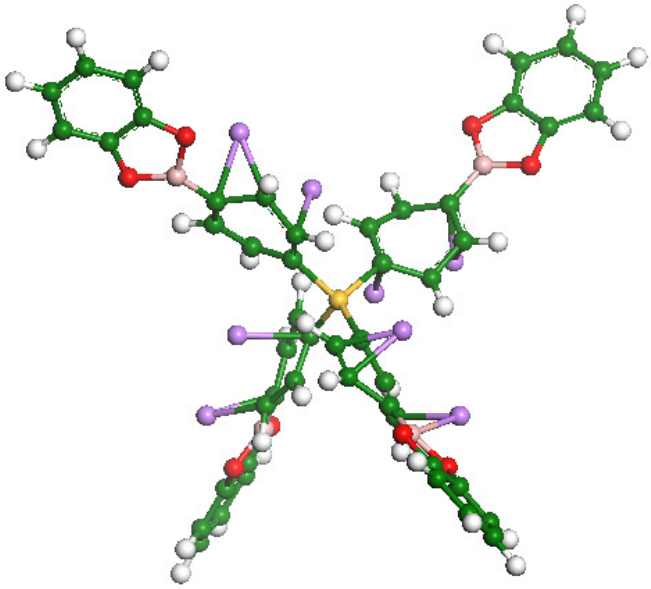

(o) Coadsorption of eight Li atoms in TBPS with part constraint

B.E. = -24.90 kcal/mol

Figure S3 Optimized adsorption sites of Li on COFs. The charge possessed by Li and the binding energies are also presented, respectively. The write, green, red, pink and violet represent H, C, O, B and Li atoms, respectively.

To evaluate the effect of Li dopants on the hydrogen storage capacity of COFs, we investigated adsorption sites of single and multiple Li atoms in COFs systematically. To gain reliable results, two big cluster models were adopted here to represent the COFs (see Figure S3). All the geometry optimizations were performed with the B3LYP/6-31G* method. The distance between the doped Li atoms and the COFs was also presented in Figure S3. Again, the binding energies, as well as the Mulliken charge possessed by per Li atom(see Figure S3), were corrected with high quality first-principles calculations, PW91/6-311g(d,p). As is well known, the Mulliken population analysis depends on the basis sets generally, and this basis set dependence is often very large. Therefore, we further verified our Mulliken population analysis results by calculating the ESP charges, derived by fitting to electrostatic potential. It is found that, for the systems studied here, the fitted ESP charges are close to those obtained from the Mulliken population analysis. The average binding energy per Li between the doped Li atoms and the COFs is defined as

$$B.E. = [\, E(nLi/subtrate) - E(subtrate) - nE(Li) \,]/n.$$

Figure S3 (a) to (n) show the optimized adsorption sites of the doped Li atoms on COFs. In our geometry optimizations, the SiH_3 group at each terminal of the cluster model was frozen to retain the constraint originated from the 3D crystal lattices. In our opinion, it is necessary to take the constraint from the lattice into consideration here, because the COFs are in crystallized state rather than being free molecules.

Figure S3 (a) to (e) show the optimized adsorption sites of a single Li atom on COFs, respectively. Our results reveal that the COFs exhibit mainly five adsorption sites for a single Li atom: (a) the hollow site in HHTP, (b) the open-hollow site in HHTP, (c) the

oxygen site in the B_3O_3 or C_2O_2B ring, (d) the hollow site in TBPM or TBPS, and (e) the open-hollow site in TBPM or TBPS. Based on our first-principles calculations, the optimum adsorption site of H_2 on the HHTP building block is the open-hollow site with the binding energy of -14.71 kcal/mol (see Figure S3 (b)), whereas that on the TBPS (TBPM) building block is the hollow site with the binding energy of -23.70 kcal/mol. The Mulliken and natural population analysis shows that the charge possessed by the doped Li atom varies in the range from 0.3 $|e|$ to 0.5$|e|$ except for the oxygen site (see Figure S3). It should be mentioned that the oxygen site is unstable, and the adsorbed Li atom migrates to the adjacent open-hollow site when coadsorbing with a H_2 molecule. In addition, when a Li atom is located on the top of the center ring in HHTP, it migrates to the open-hollow site. These results indicate that the center ring in HHTP is not an effective adsorption site for Li. Recently, Choi et al.[13] reported the metal-decorated COFs by first-principles calculations during our preparation of this paper. In their work, the binding energy between a Li cation and the COFs was calculated to be -37.35 eV by MP2/6-311++g** method, which is obviously higher than our results. The difference of their binding energies from this work can be attributed to the large basis sets adopted by them. Besides, they also evaluated the hydrogen storage of Li-doped COFs by first-principles calculations at room temperatures, and gave the predication of about 6.5 wt % for Li-doped COF-108.

Additionally, we further investigated the doping of two and more Li atoms on the TBPM, TBPS and HHTP building blocks. Figure S3 (f) to (j) display the optimized coadsorption modes for two Li atoms on COFs. As shown in Figure S3 (f), two Li atoms can be stably coadsorbed on each branch of the TBPM or TBPS building block, with one

Li atom on the top of the hydrocarbon ring, and the other on the open-hollow site, respectively. The average binding energy is approximately -23.30 kcal/mol. This is the optimum distribution for two Li atoms coadsorption on one branch, and all the other arrangements are less stable from our calculations. In addition, both of the two Li atoms are positively charged with the amount larger than $0.3|e|$. Figure S3 (g) to (j) show the optimized coadsorption modes of two Li atoms on the HHTP building block, respectively. Our calculations indicate that there are mainly four different coadsorption modes for two Li atoms on the HHTP building block. Among the four modes, those shown in Figure S3 (g) and (i) are more stable in energy, while the charge possessed by one atom in Figure S3 (g) decreases significantly. In Figure S3 (h), one Li atom is adsorbed on the substrate, while the other is far away from the substrate, due to the interaction between Li atoms. Here, the average binding energy is about -15.78 kcal/mol. Moreover, the upper Li atom is negatively charged, and the lower is slightly positively charged.

Figure S3 (k) and (l) show the optimized coadsorption modes for three Li atoms on the HHTP and TBPS building blocks, respectively. From Figure S3 (k) we can see that, when three Li atoms are placed on the top of the three outer hydrocarbon rings in the HHTP building block, they will migrate together to form a cluster with the average binding energy of about - 33.75 kcal/mol. In this case, the uppermost Li atom is negatively charged, while the other two are positively charged, due to the charge transfer between Li atoms. From Figure S3 (l) it is found that three Li atoms can also be loaded in one branch of the TBPS or TBPM building block, with the average binding energy of -38.16 kcal/mol. However, the average charge possessed by per Li decreases slightly.

Figure S3 (m) and (n) show the optimized coadsorption modes for four Li atoms on the

HHTP building block. As shown in Figure S3 (m), when three Li atoms are placed at the three open-hollow sites on one side of the HHTP, and the fourth is placed at the top of the center ring on the other side in the initial structure, the Li atoms assemble together to some extent after optimization with the average binding energy of - 38.02 kcal/mol. From Figure S3 (n) it can be found that, when three Li atoms are placed at the top of the three outer hydrocarbon rings on one side, and the fourth is placed at the top of the center ring on the other side in the initial structure, two of the Li atoms migrate to the open-hollow sites again after optimization with the average binding energy of about - 44.99 kcal/mol. In both Figure S3 (m) and (n), the charges possessed by the two Li atoms among the four are lower than $0.2|e|$. It is noticed that the average binding energy per Li atom increases significantly as the number of the doped Li atom increases, indicating the clustering tendency of multiple Li atoms.

As is well known, the neutral Li atoms or anions have no contribution to the enhancement of the hydrogen storage capacity of COFs. Therefore, to avoid unacceptable structural distortion of COFs caused by Li-doping, we only placed two Li atoms on each branch of the TBPM or TBPS building block in our following GCMC simulation, as shown in Figure S3 (f). As for the HHTP building block, we placed only one Li atom on the open-hollow site as shown in Figure S3 (b), due to the complex situations for coadsorption of multiple Li atoms. The above distribution can give reliable and moderate prediction to the hydrogen storage capacities of the Li-doped COFs.

To take into account the effect of the three neighboring C_6H_6 phenyl groups connected with Si on the adsorbed Li atoms, as shown in Figure S3 (d) and (f), we also adopted another big cluster model to evaluate the coadsorption of eight Li atoms on the TBPS

building block. Figure S3 (o) gives the optimized structure for coadsorption of eight Li atoms on the TBPS building block. In our geometry optimizations, two H atoms at the terminals of each branch of the cluster model were frozen to retain the constraint originated from the crystal lattice. It is found from our results that eight Li atoms can be loaded on the TBPM or TBPS building block theoretically. The calculated average binding energy is determined to be approximately - 24.90 kcal/mol, close to those shown in Figure S3 (d) and (f). The above results indicate that the neighboring three C_6H_6 phenyl groups connected with Si (see Figure S3 (d) and (f)) do not affect the adsorption positions of the doped Li atoms and their charge significantly.

To obtain the interaction between Li and H_2, high quality first principles calculations were performed using the PW91/6-311g(d,p) method, including the basis set superposition error correction. It can be found that this error is neglectable for our present systems studied here. Figure S4 shows the cluster model used in this work, and all the three BH terminals were kept frozen during geometry optimizations. First, we located a Li atom on the open-hollow site of the HHTP building block and performed geometry optimizations. Then, a series of single point energy calculations were carried out with the variations of the distance between H_2 and Li. Using the calculated potential energies, the force field parameters for the interaction between Li and H_2 will be determined in the next section. The calculated potential energy of Li with H_2 is presented in Figure S5.

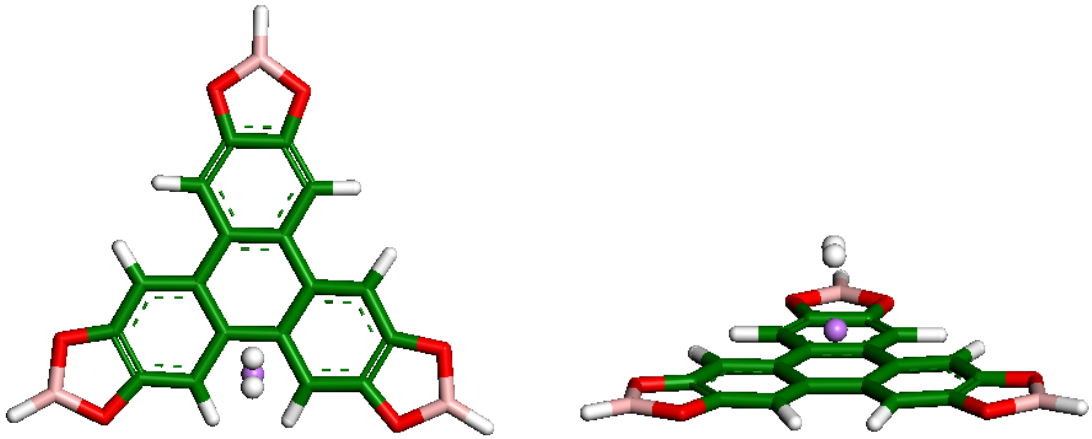

(a)Top view *(b) Side view*

Figure S4 The cluster model used to obtain the interaction between H_2 and Li doped on COF-105 (COF-108). The geometry of the Li/COF system is optimized in advance. The write, green, red, pink and violet represent H, C, O, B and Li atoms, respectively.

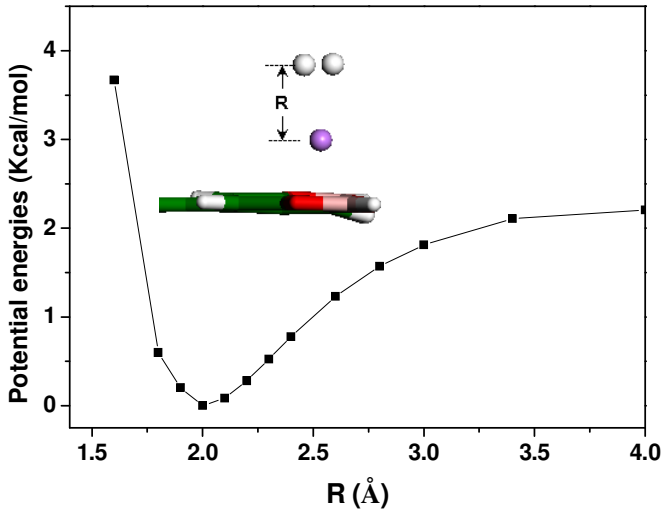

Figure S5 The potential energies as a function of the distance between Li and H_2 calculated from the first-principles calculation.

S.2 Fitting and Parameterization of the Force Field

Figure S6 (a) to (d) show the calculated potential energies used to obtain the force fields for Ar and H_2 interaction with COFs. The force field parameters for the interaction between Ar, H_2 and COFs were then determined by fitting to the following Morse potential

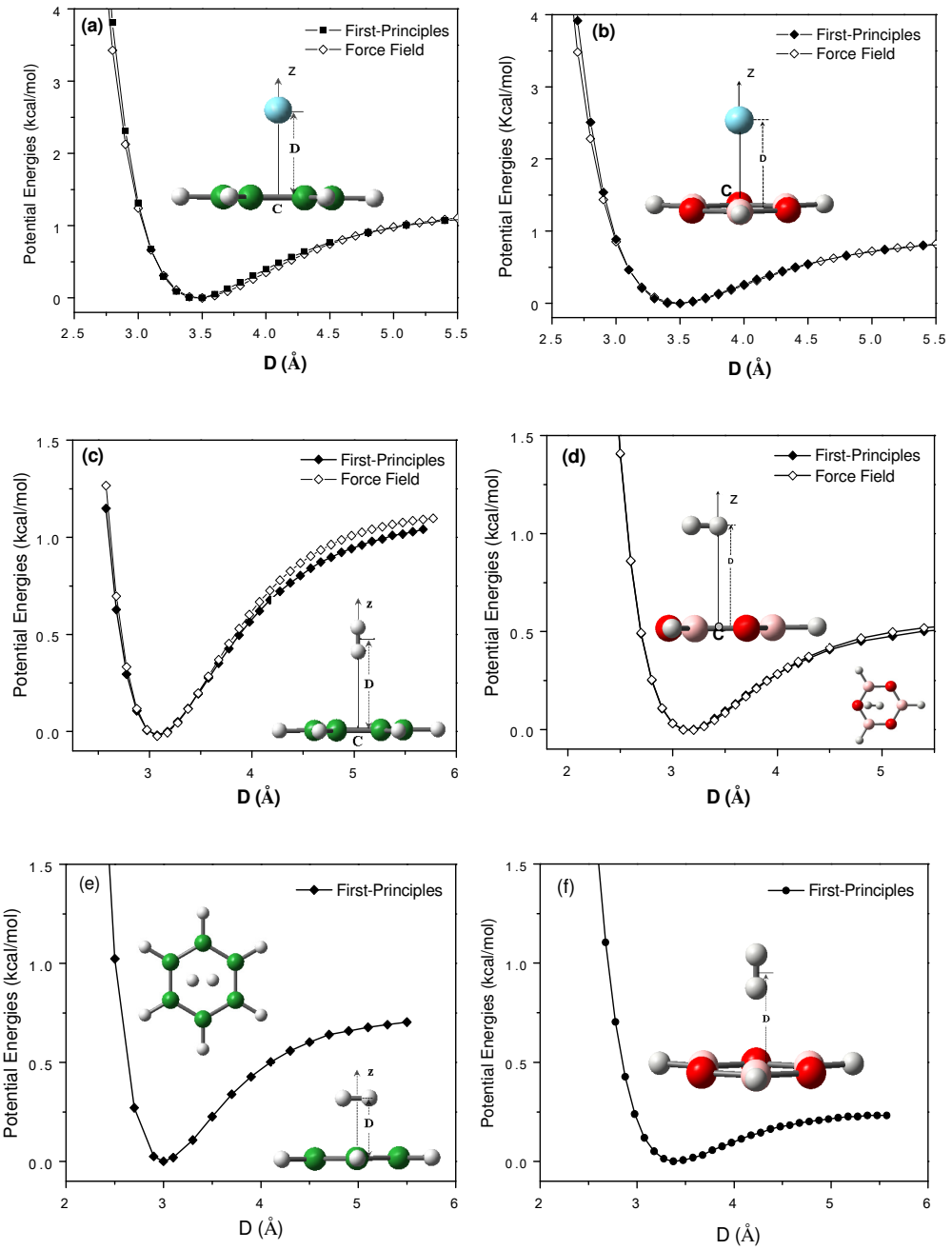

Figure S6: Potential energies derived from the first-principles calculations and our force fields, respectively. (a) Potential energy of Ar on C_6H_6. (b) Potential energy of Ar on $B_3O_3H_3$. (c) Potential energy of H_2 on C_6H_6 with its axis vertical to the plane. (d) Potential energy of H_2 on $B_3O_3H_3$ with its axis parallel with the plane. (e)Potential energy of H_2 on C_6H_6 with its axis parallel with the plane. (f)Potential energy of H_2 on $B_3O_3H_3$ with its axis vertical to the plane. The symbol C denotes the center of the C_6H_6 or $B_3O_3H_3$ plane. The definition of the distance D is shown in the snapshots.

$$U_{ij}(r_{ij}) = D[x^2 - 2x], x = \exp(-\frac{\gamma}{2}(\frac{r_{ij}}{r_e} - 1)) \qquad \textbf{(1)}$$

where r_{ij} is the interaction distance in Å. D, γ and r_e denote the well depth, the stiffness (force constant), and the equilibrium bond distance, respectively. Here, the hydrogen molecule was treated as a diatomic molecule.

The force field parameters for Ar and H_2 with H, which is bound to hydrocarbon rings, and sp^2 hybrid C, B and O were determined by the potential energies of Ar and H_2 on C_6H_6 and $B_3O_3H_3$ as presented in Figure S6 (a) to (d), derived from our first-principles calculations. It is noticed that the orientation of H_2 in the first-principles calculations has significant effect on the fitted force field. Generally, the H_2 molecule should be placed on the substrates with the adsorption-favorable orientation, which can give relatively accurate force fields and reasonable simulation results. This method was widely used in force field fitting of the non-bond interaction in previous works[12, 14] Furthermore, the force field parameters for the interaction of Ar and H_2 with four-fold coordinated C and Si atoms were determined by the binding energies of Ar and H_2 with C_5H_{12} and SiC_4H_{12}. Here, we assume that the H atoms in the four cluster models belong to one atom type. Table S2 shows the binding energies of Ar and H_2 with the four cluster models obtained from the first-principles calculations and the Morse force fields. The fitted parameters of our Morse force fields for the interaction of Ar and H_2 with COFs are shown in Table S3 and Table S4, respectively. For comparison, the fitted force fields for the interaction of Ar and H_2 with C_6H_6 and $B_3O_3H_3$ clusters are also shown in Figures S6 (a) to (d). As these clusters are the key components of COFs, and accurate representation of these units should be extendable to all COF materials. The results shown in Figure S6 indicate that the Morse potential gives an accurate representation of the potential energies obtained

from the quantum mechanics calculations.

To study the impact of H_2 orientations in first-principles calculations on the fitted force fields, we also calculated the potential energies when H_2 was orientated vertically on the $B_3O_3H_3$ plane and in parallel to the C_6H_6 plane, respectively. The obtained potential energies were presented in Figure S6 (e) and (f), respectively. It was found that when H_2 was orientated towards unfavorable orientations, the interaction between H_2 and the fragments of COFs becomes weaker significantly. It is also found that, if the potential energies obtained from unfavorable orientations of H_2 are used, the fitted force fields for the interaction between H_2 and the COFs are also significantly underestimated, correspondingly.

The force field parameters for the interaction between Li and H_2 were derived from our first principles calculations, and are presented in Table S4.

Table S2 The first-principles and Morse force field (eq.1) data on the binding energies of Ar and H_2 with the selected four cluster models used here, respectively.

□E (kcal/mol)	H_2				Ar			
	C_6H_6	$B_3O_3H_3$	C_5H_{12}	SiC_4H_{12}	C_6H_6	$B_3O_3H_3$	C_5H_{12}	SiC_4H_{12}
First-principles	-1.156	-0.575	-0.256	-0.337	-1.221	-0.967	-0.645	0.810
Force Field	-1.155	-0.568	-0.251	-0.338	-1.238	-0.983	-0.649	0.950

Table S3 Van der Waals force field parameters for non-bond interaction between Ar and COFs derived from the first-principles calculations in this work. Here, H_ denotes the H atom bound to the hydrocarbon rings.

Parameter / Atom Types [a]	D (kcal/mol)	r_e (Å)	γ
Ar---Ar [b]	0.2226	3.8720	13.0622
H_ ---Ar	0.0702	3.6500	9.0024.
C_R ---Ar	0.1661	3.8202	10.5001
B_2 ---Ar	0.1103	3.8707	11.0023
O_2 ---Ar	0.1902	3.6528	11.0023
C_3 ---Ar	0.1150	3.8202	10.0030
Si3 ---Ar	0.3250	3.9701	9.0020

[a] The first two characters correspond to the chemical symbol; an underscore appears in the second column if the symbol has one letter. The third column describes the hybridization or geometry: 1 = linear, 2 = trigonal, R = resonant, 3 = tetrahedral.
[b] The Ar---Ar force field parameters were fitted to the binding energies of two Ar atoms calculated with the CCSD(T) with aug-cc-pVQZ basis set.

Table S4 Van der Waals force field parameters for non-bond interaction between H_2 and COFs derived from the first-principles calculations in this work. H_A and H_ denote H in a H_2 molecule and H bonded to the hydrocarbon rings, respectively.

Parameter / Atom Types [a]	D (kcal/mol)	r_e (Å)	γ
H_A ---H_A [b]	0.0182	3.5698	10.7094
H_ --- H_A	0.0124	3.3001	11.0027
C_R ---H_A	0.1120	3.1800	10.5000
B_2 ---H_A	0.0328	3.6400	11.0004
O_2 ---H_A	0.0690	3.2500	11.0003
C_3 ---H_A	0.0700	3.1800	12.0062
Si3 ---H_A	0.2201	3.5200	12.0046
Li ---H_A	1.4949	2.0432	7.5672

[a] The definition rule of atom types is in accordance with that used in Table S2
[b] The force field for H_A and H_A is derived from the literature of Han et al.[12]

S.3 Adsorption isotherms

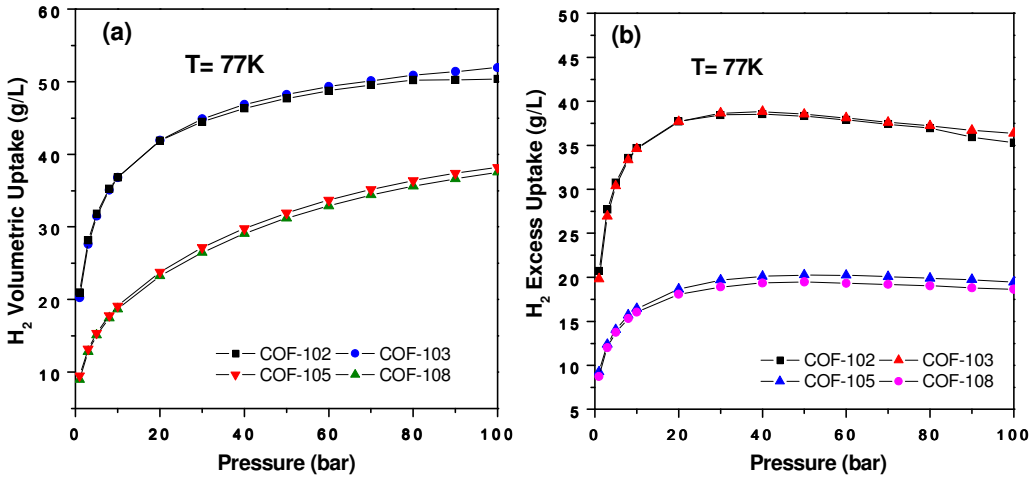

Figure S7 Adsorption isotherms of H_2 in COFs at 77 K. (a) Total volumetric isotherms. (b) Excess volumetric isotherms.

Figure S7 shows the predicted volumetric adsorption isotherms of H_2 in COFs at T=77 K by using GCMC method. It can be found from Figure S7 (a) that COF-102 and COF-103 present superior volumetric storage capacities to COF-105 and COF-108. The volumetric uptakes for COF-102, COF-103, COF-105 and COF-108 are 50.38, 51.95, 38.20 and 37.55 g/L at p=100 bar, respectively. Figure S7 (b) shows the excess adsorption isotherms of H_2 in COFs, from which we can see that COF-102 and COF-103 display the optimum volumetric adsorption capacities, 38.83 and 38.54 g/L at p=40 bar.

Figure S8 (a) and (b) show the total and excess gravimetric adsorption isotherms of hydrogen in COFs at T=298 K. The results show that COF-105 and COF-108 still exhibit high hydrogen storage capacities, in the range of 4.5 wt% ~ 4.7 wt% at T=298 K and p=100 bar. From Figure S8 (b) we can see that the excess hydrogen adsorption capacity of the COFs doesn't exceed 1.5 wt% at T= 298 K and p=100 bar. However, if the COFs are doped with Li atoms, the excess capacity of H_2 will be enhanced significantly. At T=

298 K and p=100 bar, the excess capacities of H_2 in Li-doped COF-102, COF-103, COF-105 and COF-108 reach 4.25 wt%, 4.14 wt%, 3.88 wt% and 3.90 wt%, respectively (also see Figure 4 (c) and (d) in manuscript).

From a practical point of view, the reversible storage capacity of hydrogen, i.e. the release capacity of hydrogen from the stored status at room temperatures, is important.

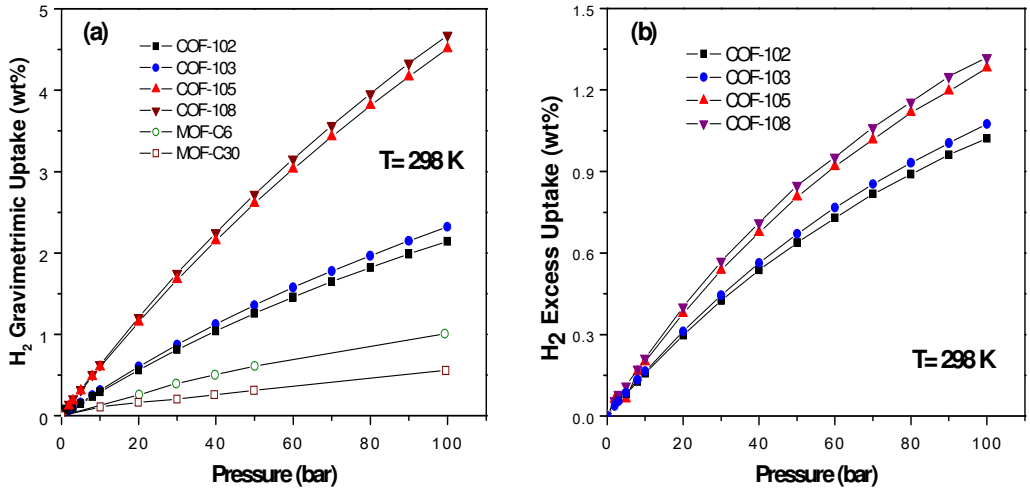

Figure S8 *Adsorption isotherms of H_2 in COFs at 298 K. (a) Gravimetric adsorption isotherms of H_2, (b) Excess adsorption isotherms. The isotherms for MOFs are also presented in (a) for comparison.*[12]

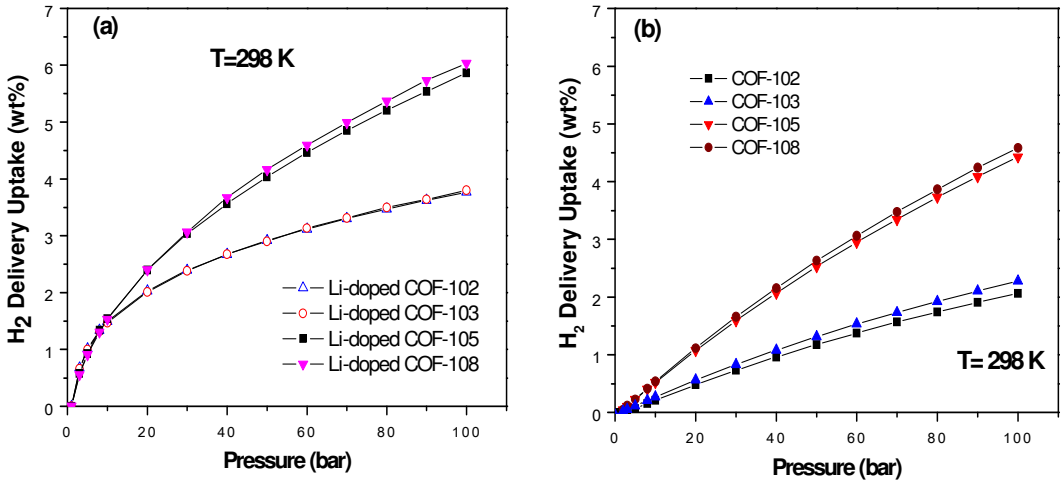

Figure S9 *Computed gravimetric delivery isotherms of H_2 in the Li-doped and non-doped COFs at T=298 K. (a) Gravimetric delivery isotherms of H_2 in the Li-doped COFs. (b) Gravimetric delivery isotherms of H_2 in COFs.*

Figure S9 presents the gravimetric delivery capacity of hydrogen in non-doped and Li-

doped COFs at T=298 K, respectively, where the delivery amount is the mass of adsorbed hydrogen at the storage or working pressure minus that at the discharge pressure p=1 bar. Although a certain part of hydrogen can not be released at the discharge pressure, the gravimetric delivery capacities of hydrogen in the Li-doped COF-105 and COF-108 still reach 5.87 and 6.03 wt% at T=298 K and p=100 bar, respectively. Compared to the non-doped COFs as shown in Figure S9 (b), the gravimetric hydrogen delivery uptakes of the Li-doped COF-105 and COF-108 can be enhanced by about 30%.

S.4 Isotherm Heat

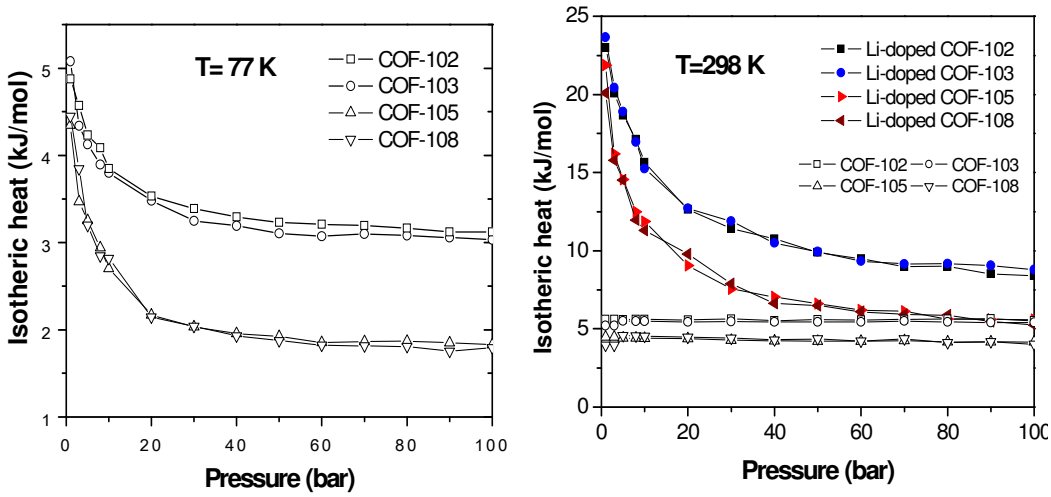

Figure S10 *Calculated isosteric heats for H_2 adsorption in pure and Li-doped COFs. (a) Isosteric heat for H_2 adsorption in COFs at T= 77 K. (b) Isosteric heat for H_2 adsorption in Li-doped COFs at T= 298 K. The isosteric heat for H_2 adsorption in COFs at T= 298 K. are also presented in (b) for*

In this part, the calculated isosteric heats are also presented. Figure S10 (a) shows the isosteric heats for H2 adsorption in COFs at T=77 K. Our results show that the isosteric heats for COF-105 and COF-108 are somewhat lower than those for COF-102 and COF-103, due to the large free volumes of COF-105 and COF-108. Most recently, Han *et al.*[14] reported their predictions on the isosteric heats of H_2 in COFs at 77 K by a simulation method, where the simulated maximum isosteric heats are 5.7 kJ/mol (COF-102), 5.8

kJ/mol (COF-103), 5.6 kJ/mol (COF-105), and 7.4 kJ/mol (COF-108), respectively. These results are comparable to this work with insignificant differences. From Figure S10 (b) we can see that the isosteric heats of hydrogen in the non-doped COFs are in the range of 4~6 kJ/mol at T=298 K. However, the isosteric heats of hydrogen in the Li-doped COFs are evidently larger due to the strong interaction between H_2 and the doped Li cations. The calculated maximum isosteric heats of H_2 in Li-doped COFs at T=298 K are 22.99 kJ/mol (COF-102), 23.66 kJ/mol (COF-103), 21.88 kJ/mol (COF-105), and 20.09 kJ/mol (COF-108), respectively. These results coincide with the first-principles calculations in this work and in the literature, where the binding energy of H_2 with a Li cation is within the range of 2~5 kcal/mol (~ 21 kJ/mol). [15, 16]

In the literature,[17] it is pointed out that the optimal interaction energies should be in the range between physisorption and chemisorption. In this case, the hydrogen stored in the host material could be released reversibly at room temperature. Our results show that for the Li-doped COFs, the interaction between H_2 and the host materials is significantly strengthened, which is much larger than that for physisorption in microporous materials. This may be the reason why the Li-doped COFs exhibit an excellent hydrogen storage performance at room temperature.

References

[1] H. M. El-Kaderi, J. R. Hunt, J. L. Mendoza-Cortes, A. P. Cote, R. E. Taylor, M. O'Keeffe, O. M. Yaghi, *Science* **2007**, *316*, 268.

[2] M. J. Frisch, G. W. Trucks, H. B. Schlegel, G. E. Scuseria, M. A. Robb, J. R. Cheeseman, J. A. Montgomery, Jr., T. Vreven, K. N. Kudin, J. C. Burant, J. M. Millam, S. S. Iyengar, J. Tomasi, V. Barone, B. Mennucci, M. Cossi, G. Scalmani, N. Rega, G. A. Petersson, H. Nakatsuji, M. Hada, M. Ehara, K. Toyota, R. Fukuda, J. Hasegawa, M. Ishida, T. Nakajima, Y. Honda, O. Kitao, H. Nakai, M. Klene, X. Li, J. E. Knox, H. P. Hratchian, J. B. Cross, C. Adamo, J. Jaramillo, R. Gomperts, R. E. Stratmann, O. Yazyev, A. J. Austin, R. Cammi, C. Pomelli, J. W. Ochterski, P. Y. Ayala, K. Morokuma, G. A. Voth, P. Salvador, J. J. Dannenberg, V. G. Zakrzewski, S. Dapprich, A. D. Daniels, M. C. Strain, O. Farkas, D. K. Malick, A. D.

Rabuck, K. Raghavachari, J. B. Foresman, J. V. Ortiz, Q. Cui, A. G. Baboul, S. Clifford, J. Cioslowski, B. B. Stefanov, G. Liu, A. Liashenko, P. Piskorz, I. Komaromi, R. L. Martin, D. J. Fox, T. Keith, M. A. Al-Laham, C. Y. Peng, A. Nanayakkara, M. Challacombe, P. M. W. Gill, B. Johnson, W. Chen, M. W. Wong, C. Gonzalez, J. A. Pople, revision B.02 ed., Gaussian, Inc., Wallingford, CT.

[3] C. Lee, W. Yang, R. G. Parr, *Phys. ReV. B,* **1988**, *37*, 785.

[4] A. D. Becke, *J. Chem. Phys.* **1993**, *98*, 5648.

[5] J. P. Perdew, Y. Wang, *Phys. Rev. B* **1992**, *45*, 13244.

[6] M. J. Frisch, M. Head-Gordon, J. A. Pople, *Chem. Phys. Lett.* **1990**, *166*, 275.

[7] M. J. Frisch, M. Head-Gordon, J. A. Pople, *Chem. Phys. Lett.* **1990**, *166*, 281.

[8] M. Head-Gordon, T. Head-Gordon, *Chem. Phys. Lett.* **1994**, *220*, 122.

[9] M. Head-Gordon, J. A. Pople, M. J. Frisch, *Chem. Phys. Lett.* **1988**, *153*, 503.

[10] D. E. Woon, T. H. Dunning Jr., *J. Chem. Phys.* **1993**, *98*, 1358.

[11] R. A. Kendall, T. H. Dunning Jr., R. J. Harrison, *J. Chem. Phys.* **1992**, *96*, 6796.

[12] S. S. Han, W. A. Goddard, III, *J. Am. Chem. Soc.* **2007**, *129*, 8422.

[13] Y. J. Choi, J. W. Lee, J. H. Choi, J. K. Kang, *Appl. Phys. Lett.* **2008**, *92*, 173102.

[14] S. S. Han, H. Furukawa, O. M. Yaghi, W. A. Goddard, III, *J. Am. Chem. Soc.* **2008**, *130*, 11580.

[15] A. Mavrandonakis, E. Tylianakis, A. K. Stubos, G. E. Froudakis, *J. Phys. Chem. C* **2008**, *112*, 7290

[16] W.-Q. Deng, X. Xu, W. A. Goddard, *Phys. ReV. Lett.* **2004**, *92*, 166103.

[17] R. C. Lochan, M. Head-Gordon, *Phys.Chem. Chem. Phys.* **2006**, *8*, 1357.